Since January 2020 Elsevier has created a COVID-19 resource centre with free information in English and Mandarin on the novel coronavirus COVID-19. The COVID-19 resource centre is hosted on Elsevier Connect, the company's public news and information website.

Building and Environment 204 (2021) 108131

Contents lists available at ScienceDirect

Building and Environment

journal homepage: www.elsevier.com/locate/buildenv

COVID-19 and urban spaces: A new integrated CFD approach for public health opportunities

Asmaa M. Hassan *, Naglaa A. Megahed

Architectural Engineering and Urban Planning Department, Faculty of Engineering, Port Said University, Port Said, Egypt

ARTICLE INFO

Keywords:
Transmission of COVID-19
Urban public spaces
Urban seats
Coughing droplets
Deposition fraction
CFD simulation

ABSTRACT

Safe urban public spaces are vital owing to their impacts on public health, especially during pandemics such as the ongoing COVID-19 pandemic. Urban public spaces and urbanscape elements must be designed with the risk of viral transmission in mind. This work therefore examines how the design of urbanscape elements can be revisited to control COVID-19 transmission dynamics. Nine proposed models of urban public seating were thus presented and assessed using a transient three-dimensional computational fluid dynamics (CFD) model, with the Eulerian–Lagrangian method and discrete phase model (DPM). The proposed seating models were evaluated by their impact on the normalized air velocity, the diameter of coughing droplets, and deposition fraction. Each of the proposed models demonstrated an increase in the normalized velocity, and a decrease in the deposition fraction by >29%. Diagonal cross linear and curved triangle configurations demonstrated an improved airflow momentum and turbulent flow, which decreased the droplets deposition fraction by 68%, thus providing an improved, healthier urban public seating option.

1. Introduction

Global urbanization, increased urban population density of cities, and increased environmental issues caused by anthropogenic activities have contributed to global human health issues [1–5]. One such issue, the shortage of health care services in megacities, has contributed to difficulties controlling global health crisis [6]. Consequently, COVID-19 dramatically spread worldwide in late 2019 [7–14], owing to its viral transmission ability [15–18] through direct or indirect contact [19–21], has thus significantly impacted health care, social, commercial, and industrial activities [22–26].

The World Health Organization (WHO) declared the COVID-19 epidemic a public health emergency of international concern of "alarming levels of spread and severity" [9,14,23,27–29]. COVID-19 can be transmitted through respiratory droplets, particles >5–10 μm in diameter, and droplet nuclei, particles <5 μm in diameter [30]. Droplet transmission occurs directly via the inhalation of respiratory droplets or when exhaled droplets (from exhaling reach either the mucosae; mouth, and nose, or eyes of another person, through breathing, coughing, sneezing, or talking) reach the mucosae of the mouth, nose, or eyes [15, 30,31]. Indirect transmission can also occur, in which the virus is deposited or contaminated on surfaces and then transferred via subsequent hand-to-mouth, nose, or eye actions [9,15,27].

To mitigate the spread of COVID-19, many local and global procedures have been recommended that have heavily impacted daily life [13,27,31–35]. The WHO called on all countries to reduce transmission through specific steps like: detect, test, treat, isolate, trace, and mobilize citizens [33]. Consequently, countries have moved to implement these steps through strict protocols [27,33] that have presented challenges a wide variety of fields [36–40].

To begin addressing these issues, Ai et al. (2020) and Dudalski et al. (2020) aimed to clarify the process of airborne transmission, i.e., how infectious droplet nuclei can spread and remain suspended in the air, which contribute in the transmission of COVID-19, based on the air velocity, and particle size [41]. Others have applied this process to clarify how individuals can minimize the probability of infection in public spaces [27,33,42,43], for instance, by implementing social distancing guidelines and using facial masks and shields [4,44–46]. Consequently, many governments have announced social distancing guidelines to promote social relationships and escape household confinement while maintaining distances of 1–2 m, including in Australia, Qatar, USA, Canada, Spain, UAE, UK, New Zealand, Italy, and South Korea [47,48]. Microclimate airflow in urban public spaces has also been reviewed [49,50], as has the importance of variable ambient

* Corresponding author. Tel.: +2001112862511.
E-mail addresses: assmaa.mohamed@eng.psu.edu.eg (A.M. Hassan), naglaaali257@hotmail.com (N.A. Megahed).

https://doi.org/10.1016/j.buildenv.2021.108131
Received 27 May 2021; Received in revised form 29 June 2021; Accepted 7 July 2021
Available online 12 July 2021

air, evaporation, and turbulent flow for runners and cyclists on COVID-19 transmission patterns, to further clarify social distancing requirements [20,46,48,51].

Hollander (2020) asserted that the COVID-19 pandemic promotes the significance of urban public spaces, implicating current urban designs and future architectural and urban design research [52–54]. Planners, and architects thus have the unique opportunity to build and develop more resilient open spaces, and equitable urban communities, which can promote inequality through design outdoor spaces, which promote residents' lives [39,55–57]. Consequently, researchers worldwide have discussed the urgent need for designing and planning open spaces in response to COVID-19 around the world, which are important social and ecological determinants in high-density cities that provide residents with the opportunity for physical activity, mental innovation, social health, and improves overall wellbeing [33,58–60], as well as improve the city's air temperature and quality [60–63]. Honey-Rosés et al. (2020) discussed among planners, designers, architects, urbanscape managers how this pandemic will lead to a revisiting of residents' relationship with public spaces. Megahed and Ghoneim (2020) and Ronchi and Lovreglio (2020) both emphasized the importance of horizontal extension with more available open spaces, which may prevent the spread of infections and diseases. Further, Gouveia and Kanai (2020), Hollander (2020), Rice et al. (2020), and Samuelsson et al. (2020) declared how social behavior in urban public spaces can be considered a source of resilience, where people can enjoy urban spaces and socialize while following social distancing guidelines to reduce COVID-19 transmission.

However, the design of urbanscape elements in such places, including seating design, to reduce transmission of infectious diseases has not yet been adequately investigated. This work therefore aims to examine urban public seating configurations and their impact on COVID-19 transmission using computational fluid dynamics (CFD) model. To do so, a computational model is proposed, verified, and then applied to a case study, as summarized in (Fig. 1).

The methodology and computational design of these studies are presented in Section 2; the results are then presented and analyzed in Section 3. An in-depth discussion of the impact of design configurations studied and backrest placement is then presented in Section 4 before concluding remarks are detailed in Section 5.

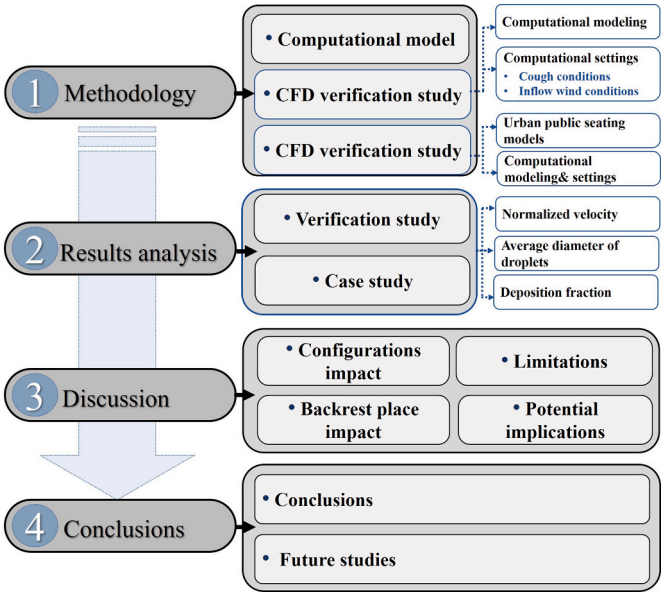

Fig. 1. Roadmap of further study structure.

2. Methodology

Building upon advances in computational resources, in particular CFD, an integrated modeling approach using numerical modeling [64] is employed to investigate the influence of the design of urban public seats on COVID-19 transmission in urban public spaces. CFD has been applied in a wide variety of fields, engineering flow analysis, building structure design, urban wind flow prediction, and air pollution dispersion to urban design, and urbanscape planning [65,66], enabling urbanscape designers, urban designers, and planners to develop design alternatives [67–69]. Further, researchers have recently discussed, and used CFD to simulate the flow behavior, transition, and the deposition of COVID-19 [7,70], such as the transmission, evaporation, and airflow around COVID-19 droplets emitted by exhaling walkers or runners examined by Blocken et al. (2020a). Here, a numerical model based on transient CFD simulations is developed to investigate the influence of urban public seating configurations on the transmission of COVID-19. A CFD verification study is then performed to confirm the reliability of the proposed model. The computational settings including boundary conditions, computational domain, meshing size, and turbulence model are established.

2.1. Computational model

The numerical model was developed using Ansys Fluent (Ansys, Inc. Canonburg, PA, USA) for three-dimensional (3D) transient-state simulations. The 3D Eulerian–Lagrangian method for multiphase flow was employed. The 3D Eulerian method can simulate realistic outdoor airflow conditions using the governing equations as follows:

$$\frac{\partial u_j}{\partial x_j} = 0 \tag{1}$$

$$\frac{\partial u_i}{\partial t} + u_i \frac{\partial u_i}{\partial x_j} = \frac{1}{\rho}\frac{\partial p}{\partial x_i} + \frac{1}{\rho}\frac{\partial \tau_{ij}}{\partial x_j} + g_i \tag{2}$$

where (u_j) represents the fluid velocity, (p) is the ambient pressure, $g_i = 9.81\ \mathrm{ms}^{-2}$ is the gravitational constant aligned in the positive x-direction, and (τ_{ij})presents the viscous stress tensor, which can be expressed as

$$\tau_{ij} = \mu\left[\frac{\partial u_i}{\partial x_j} + \frac{\partial u_j}{\partial x_i} - \frac{2}{3}\delta_{ij}\frac{\partial u_k}{\partial x_k}\right] \tag{3}$$

3D Reynolds-averaged Navier–Stokes (RANS) equations with RNG k-epsilon turbulence model were employed, as recommended by Refs. [71–73]. Here the turbulent kinetic energy (K), and turbulent dissipation rate $(\boldsymbol{\varepsilon})$ can be respectively expressed as

$$K = \frac{U_j^2}{\sqrt{C_\mu}}\left(1 - \frac{z}{\delta}\right) \tag{4}$$

$$\varepsilon = \frac{U_j^3}{Kz}\left(1 - \frac{z}{\delta}\right) \tag{5}$$

where (z) represents the height, (δ) presents the boundary layer depth, and the Von Kàrmàn constant (K) and $(C\mu)$ were set to 0.40 and *0.09* respectively.

The 3D Lagrangian method can also be used to examine the transport of cough droplets [74,75]. A Discrete Phase Model (DPM) can be used to track the transmission of COVID-19 in urban public spaces emitted from a cough, a most common respiratory activity, via the cough flow field, droplet transport, and size change and deposition of the emitted droplets. The governing equation of the 3D Lagrangian method with a DPM was defined as:

$$\frac{d}{dt}\left(m_d u_{d,i}\right) = F_i^D + F_i^L + F_i^{BM} + F_i^G \tag{6}$$

while (F_i^D), (F_i^L), (F_i^{BM}), and (F_i^G) represent the drag force, lift force, Brownian motion-inducted force, and gravity respectively. Here, (F_i^D) can be defined as

$$F_i^D = \frac{1}{8}\pi\rho d_d^2 C_D(\vec{u} - \vec{u_d}) - |\vec{u} - \vec{u_d}| \Big/ C_c \tag{7}$$

where (d_d) is the diameter of the droplet, (C_c) presents the Cunninggham correction factor, and (C_D) is the drag force coefficient, which can be expressed as:

$$C_D = a_1 + \frac{a_2}{R_{e_d}} + \frac{a_3}{R_{e_d}^2} \tag{8}$$

While the constants (a_1), (a_2), and (a_3) are calculated by the Reynoholds number of the droplet. As (F_i^{BM}), just droplets evaporate into small sizes, its value can be considered significant. While according to the condensation, and evaporation of water vapor in both of ambient air, and the cough droplet, the mass, and energy balance for each droplet can be expressed as

$$\frac{dm_d}{dt} = -\sum_{e=1}^{k}\int_{surf} n_e dA \approx -\sum_{e=1}^{k}(\overline{n_e} \times A) \tag{9}$$

$$\overline{n_e} = \frac{\rho_g Sh \widetilde{D_e} C_m}{d_d} \ln\frac{1 - Y_{e,\infty}}{1 - Y_{e,surf}} \tag{10}$$

here k = 1 for water, and ($\overline{n_e}$) represents the average mass flux of evaporable component (e) on the surface, and can be determined by:

in which (ρ_g) presents the density of the ambient air, ($Y_{e,\infty}$), and ($Y_{e,surf}$) present the mass fractions of evaporable component (e) in the gas phase far from the droplet, and on droplet surface respectively, as well the Sherwood number (Sh) can be calculated by:

$$Sh = \sqrt[3]{1 + Re_d \times \quad \mathrm{Sc} \times \quad max[1, Re_d^{0.077}]} \tag{11}$$

while $\mathrm{Sc} = \frac{\mu}{\rho D_e}$ is the Schmit number, and D_e express the mass diffusivity of component (e). Furthermore, (C_m) is Fuchs-Knudsen number correction, which determined by the following formula:

$$C_m = \frac{1 + Kn}{1 + \left(\frac{4}{3\alpha_m} + 0.377\right)Kn + \frac{4}{3\alpha_m}Kn^2} \tag{12}$$

where the Knudsen number $Kn = 2\lambda/d_d$, (λ) is the ratio between the diffusion coefficient of water vapor, the mean thermal velocity of the condensing water vapor, and (α_m) presents the mass thermal accommodation coefficient. In addition, ($Y_{e,surf}$) can be calculated as

$$Y_{e,surf} = y_e x_e K_e \frac{P_{ve.sat}(T_d)}{\rho R_e T_d} \tag{13}$$

in which (y_e) presents the activity of component (e), (x_e) is the mole fraction of (e) in the droplet, (R_e) is gas constant, (T_d) express the droplet temperature, $P_{ve.sat}(T_d)$ is the saturation pressure of component (e) at temperature (T_d), and (K_e) is the correction factor for the Kelvin effect, which can be calculated as

$$K_e = \exp\left(\frac{4\sigma M_e}{R\rho_d d_d T_d}\right) \tag{14}$$

while (σ) presents the surface tension of the droplet, (M_e) is the molar mass of component (e), (R) is the universal gas constant, as well (ρ_d) is the droplet density.

Finally, the energy balance equation can be determined by the followings:

$$\sum_{i=1}^{m} m_{d,i} c_{d,i} \cdot \Delta T = \pi d_d \lambda_g Nu(T_\alpha - T_d) - \sum_{e=1}^{k}\iint_d n_e L_e dA \tag{15}$$

where (Nu) represents the Nusselt number, calculated as

$$Nu = (1 + Re_d Pr)^{1/3} max\left[1, Re_d^{0.077}\right] \tag{16}$$

where (Re_d) is the Reynolds number of the droplet, and (Pr) represents the Prandtl number.

2.2. CFD verification study

Several researchers have developed and verified experimental studies and numerical models related to the transmission of COVID-19 droplets through coughing and sneezing, as summarized in (Table 1). Such studies and models focused on the transmission of COVID-19 droplets during various conditions and states, which proposed wealth resources for many applications. This study analyzed these studies according to their method of analysis, state of simulation, validation and state of human. Therefore the authors selected [76] for its diversity in inflow conditions including the wind velocity, relative humidity, and wealth findings during time sequence in outdoor spaces.

2.2.1. Computational modeling

As presented in (Fig. 2), two humans in a cuboid space located 1.83 m apart were modeled. A cough droplets is simulated by having, the mouth of the human on the left open with a hydraulic diameter equal of 10 mm, as detailed by Ref. [76].

2.2.2. Computational settings

With regard to the boundary conditions, the cough droplets are injected from the mouth of the virtual human on the left. The left and right planes of the domain represent a velocity inlet and a zero gradient pressure outlet respectively. Symmetry boundary conditions were set at the last three side planes, as presented in (Fig. 2). According to the computational settings (Table 2), the verification and case study assembled in cough conditions, as outlined in Ref. [76], and the temperature of ambient air.

On the other hand, the case study focused on only the inflow wind velocity of 5.5 m/s, temperature of 27 °C and 40% relative humidity among the inflow conditions of verification study to simulate summer time in Delta and Cairo region in Egypt. It's worth mentioning that the inflow direction was perpendicular to humans in both verification and case study.

Table 1
Literature review of modeled COVID-19 transmission via droplets expelled during coughing and sneezing.

Space	References	Method	Solution CFD state	Validated with	Human status
Outdoor spaces	[20]	Simulation& Wind tunnel experiment	Steady	[77,78]	Running
	[76]	Simulation	Transient	[79–82]	Standing
	[83]	Simulation	Steady	———	Walking
	[70]	Simulation	Steady	[84]	Standing
Indoor spaces	[85]	Simulation& Cough chamber experiment	Transient	———	Sitting
	[8]	Simulation	Steady	[86]	Sitting
	[87]	Simulation	Steady	[88]	Sitting
	[89]	Simulation	Transient	[87]	Sitting

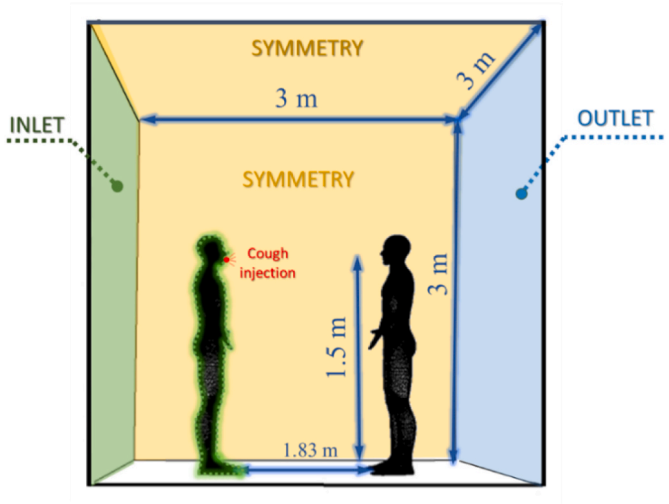

Fig. 2. Schematic of boundary conditions and domain dimensions of verification study. Source the authors after [76].

2.3. Case study

As urban spaces have been increasingly rediscovered owing to COVID-19 lockdown, the importance of urban public spaces [90] and in particular, the design of urbanscape elements, to promote social behaviors has increased. Whereas urban public spaces, including parks, streets, squares, and pedestrian areas, can host vibrant functions, which promote the character of cities and the quality of life [91–95]. In addition, urban public spaces can be realized as a vital constituent of the cities and an important social determinant of physical and mental health [59,61,63,96]. However, the safety of such spaces must be analyzed, as wearing face coverings may be difficult in some situations, as detailed by Sakharov, and Zhukov (2020). Further, various configurations of constructions such as buildings, kiosks, and other urbanscape elements can promote vortex formation, turbulence intensity and impact the air quality [97–101], and promote urban ventilation, which in turn influences the transmission of COVID-19. Thus, to contribute to the design of a safe environment that promotes health and wellbeing, the authors have fixed the computational modeling, and settings of urban space to computationally assess the design of proposed urban public seating models according to their COVID-19 transmission dynamics.

2.3.1. Urban public seating models

The nine proposed models of benches were compared with the common model of traditional urban public benches, shown in (Fig. 3), which is 1.50 m in length, 0.50 m in width, and 0.50 m in height with a one-way backrest that in many cases cannot provide a safe physical distance between individuals, or eddies of ambient air. As the linear shape of bench with specified backrest enables sitting next to each other in one direction without committing to social distances, besides decreasing the ability of air ventilation owing to weak eddies of ambient air.

The design of nine proposed models aims to promote both recirculation regions through increased localized airflow momentum and turbulence intensity. As a result, air velocities can be enhanced, which subsequently can impact on the transmission of COVID-19. The nine proposed models of benches can be defined based on three main criteria, as summarized in (Table 3): shape (linear or centered), number of sides (3–8), and rotation. With respect to models one to four, the diagonal linear shapes represented the main form. As the first model based on three symmetric diagonal cross linear shape, with similar angles, which provides air eddies. Also, model two resembles the first one with inversed direction, and circular seats. Additionally, four symmetric diagonal cross linear seats were provided in model three, besides a horizontal seat as a divider between four crossed linear seats was presented in model four.

On the other hand, the models from five to nine depended on the central shapes. Models five, and six included tripartite form, like a triangle, and parabola shape. Otherwise, the hexagonal, octal, and circular central forms were provided in the seventh, eighth, and ninth models respectively.

2.3.2. Computational modeling, and settings

In accordance with vertical and lateral guidelines to keep the blockage ratio below 3%–5% as recommended by Refs. [102,103], the computational domain was set to 43.8 × 12 × 8.8 m^3 (length, width, height, respectively), as shown in (Fig. 4). As outlined in (Table 2), an inflow wind velocity of 5.5 ms^{-1}, temperature of 27 °C and relative humidity of 40% were selected to simulate summer time in Delta and Cairo region in Egypt. It's worth to mention that the perpendicular inflow direction in case study includes both traditional and proposed urban public benches, which reflects significant impact on the localized airflow momentum and turbulence intensity hence COVID-19 transmission.

A mesh independence study and time step analysis were first

Table 2
Computational settings of verification, and case study. Source the authors after [76].

		Verification study	Case study
Solver settings		**3D transient RANS equations with the commercial CFD code Fluent in Ansys software**	
Domain		**3 × 3 × 3 m^3**	**43.8 × 12 × 8.8 m^3**
Cough	Temperature	**37°C**	
	Droplets' diameters	**2: 2000 μm**	
	Ingredients	**10.4% NaCl & 89.6% water**	
Inflow	Air velocity	**V = 0, 1, 3.9, & 5.5 m/s**	V = 5.5 m/s
	Temperature	**27°C**	
	Relative humidity	**RH = 40% & RH = 99.5%**	RH = 40%
Mesh		**High-resolution hexahedral grid meshes were generated using Ansys 14.5 Meshing. The minimum dimension of cells equals:**	
		0.0001 m	**0.001 m** owing to a mesh independence study
		in regions close to the injection of COVID-19 droplets, with a growth rate of less than 1.2 between sequential cells. The final number of the computational cells:	
		3,257,192 cells	**1,075,552 cells**
Time duration		**Intel (R) Core (TM) i7-7700 CPUs, 3.60 GHz processors, and 32 GB of RAM memory per computer used to simulate 0.4 s, every numerical simulation occupied approximately:**	
		72 h with a time step = **0.0001 s**	140 h with a time step = **0.001 s**, due to time step analysis
Measuring points		**The point of respiratory organs of**	
		standing humans, at **1.5 m** high	sitting humans, at **1.1 m** high

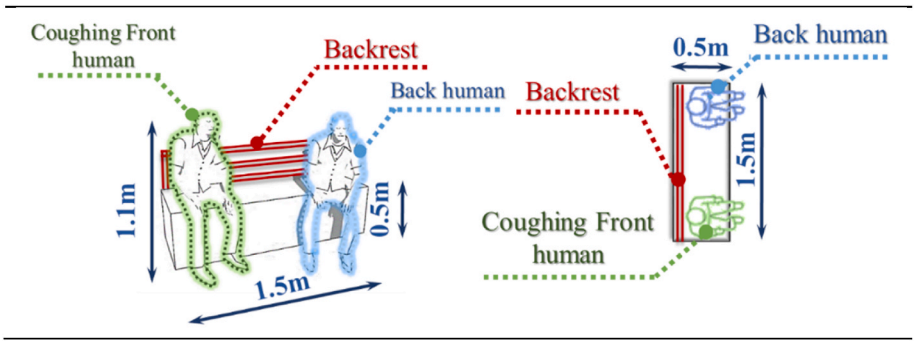

Fig. 3. The common model of traditional urban public benches.

Table 3
Proposed models of urban public seats.

Model (M.)	Shape	Rotation	No. sides	Illustration Scale: 1/100
1	Linear	Diagonal	**3**	 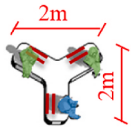
2				 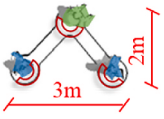
3			**4**	 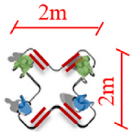
4		Diagonal/Perpendicular	**5**	 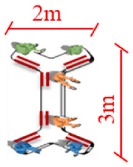
5	Centered	Paralel	**3**	 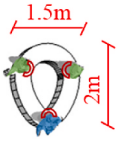
6				 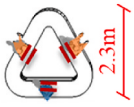
7			**6**	 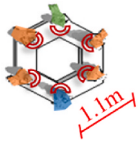
8			**8**	 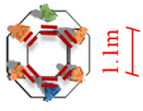
9		Paralel/Perpendicular	∞	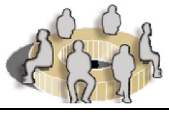 

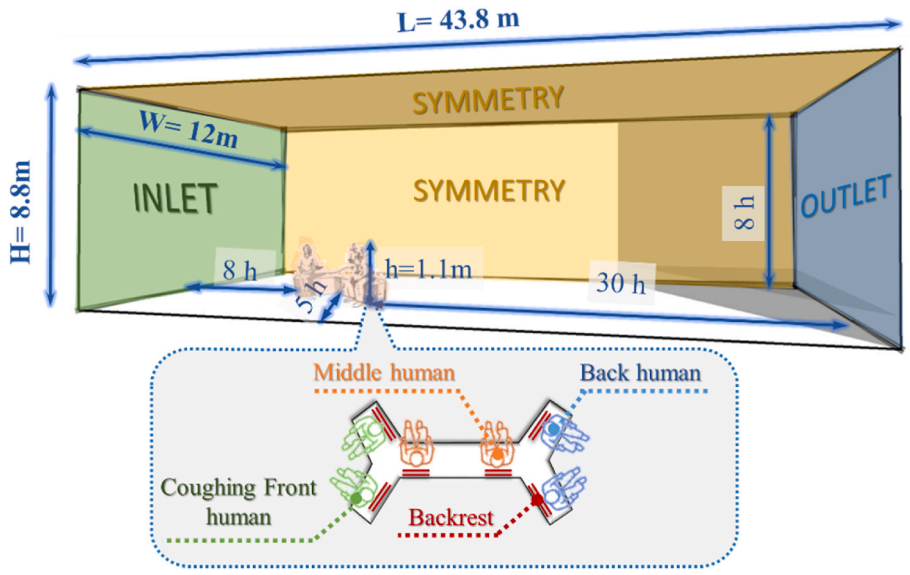

Fig. 4. Schematic of boundary conditions and domain dimensions of the case study with seated humans and their backrests.

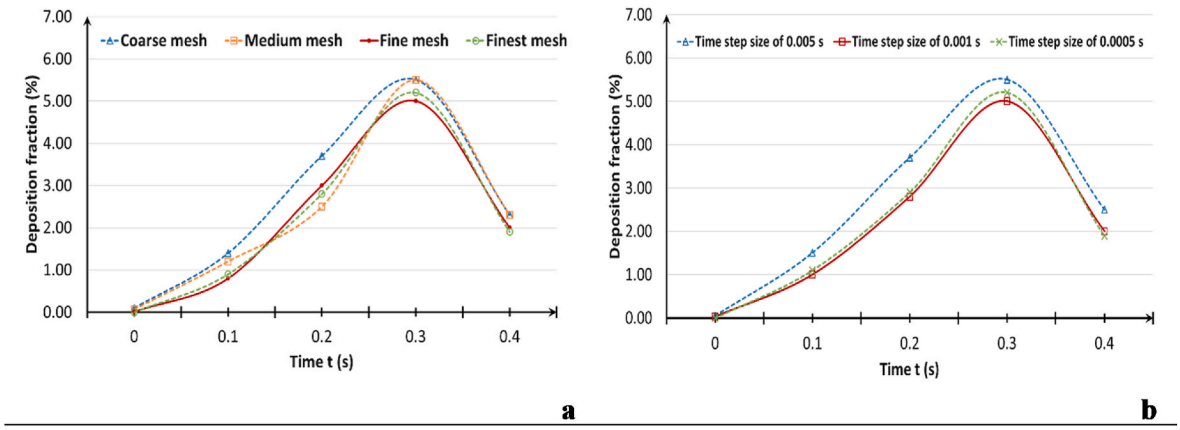

Fig. 5. Variation in deposition fraction on the right human when varying the a) mesh size, using a time step of 0.001 s, and b) the time step, using a fine mesh.

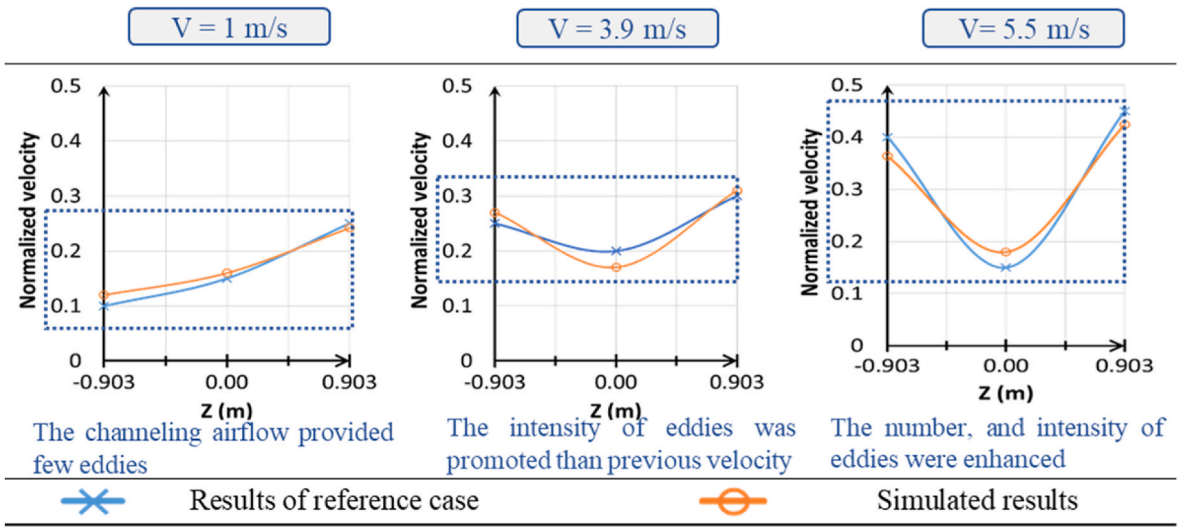

Fig. 6. Normalized velocity of verification study. Source the authors after [76].

performed using coarse, medium, fine, and superfine meshes, and time steps of 0.005, 0.001, and 0.0005 s, respectively; the results are summarized in Fig. 5, respectively. No significant differences were observed in the deposition fraction based on the fine and superfine meshes. Only negligible differences were observed in the deposition fraction when time steps of 0.005 and 0.001 s were used. Therefore, a fine mesh with a grid size of 0.001 m and a time step of 0.001 s were selected for further numerical simulation.

3. Results analysis

In this section, the results of the CFD verification study and the case study are presented and analyzed in terms of normalized air velocity, the average diameter of suspended droplets after a cough (d_d), and deposition fraction of cough droplets.

3.1. Results of verification study

The calculated normalized air velocity was in good agreement overall with the reference data, as shown in (Fig. 6). The approaching wind provided airflow to channel towards the infected human, which impacted eddies and thus the normalized air velocity near the healthy human. At an air velocity of 1 m/s, the channeling airflow provided few eddies near the left human, thus leading to a low normalized air velocity near the right human. Increasing the air velocity to 3.9 m/s and then again to 5.5 m/s increased the intensity of eddies and thus increased the normalized air velocity near the right human.

Good agreement was also observed for the average diameter of suspending droplets in the 0–0.40 s time sequence at both relative humidity levels (40% and 99%), as shown in (Fig. 7). At the lower humidity level, the average diameter of the droplets decreased with time, whereas that at the higher humidity level increased with time.

The resulting percentage of droplet deposition from the reference and simulated cases proposed model were also in good qualitative agreement for both relative humidity levels and all wind velocities

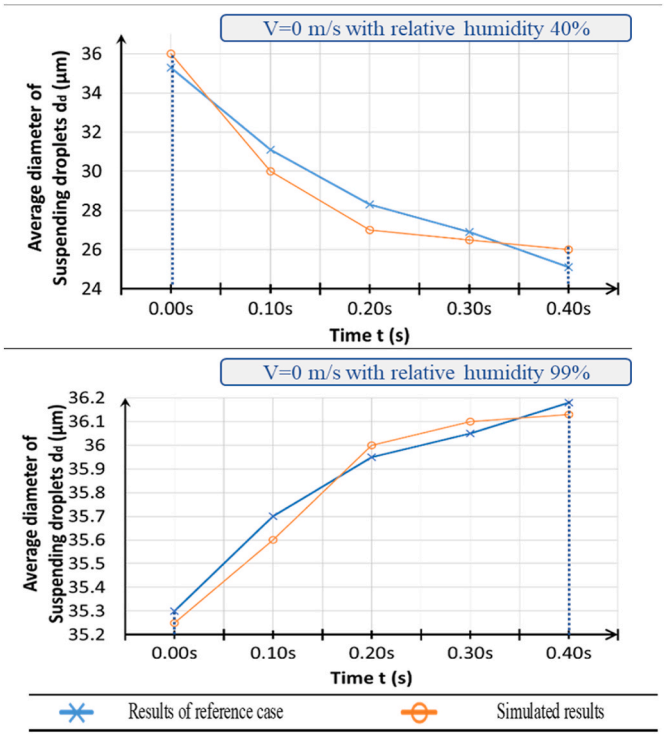

Fig. 7. Average diameter of suspending droplets of verification study. Source the authors after [76].

studied, as shown in (Fig. 8). The percentage of deposited droplets varies with the position of the coughing human, wind velocity, and relative humidity. With an increasing wind velocity, the deposition fraction gradually increased on the left coughing human, whereas on the ground, the deposition fraction gradually decreased with increasing wind velocity, and the deposition fraction on the right healthy human fluctuated and lastly decreased at 5.5 m/s.

3.2. Results of case study

The nine proposed urban seating models were then examined using the three parameters; normalized velocity, the average diameter of cough suspending droplets and percent of deposition fraction.

The resulting trends of normalized air velocity, which promotes air vortex and thus affects COVID-19 transmission, are shown in (Fig. 9). In this context, this study calculated the normalized of air velocity by dividing the air velocity in the proposed seating model by that in the common case, as several studies were based on normalized values to highlight the impact of variables, as calculated in Refs. [70,76,104]. The normalized velocity was higher than the baseline value (1.0) in each of the nine proposed seating configurations, thus demonstrating their influence in providing the vertical transmission of COVID-19 instead of only the horizontal transmission, in addition to the vertical turbulent shear intensification.

The normalized air velocity near the front coughing human significantly exceeded the baseline value in all models except model eight, where wake flow caused a near-baseline value. Further, the normalized air velocity near this human reached nearly 5.0 in models three, four, and five, owing to the increased upwind ventilation and turbulent flow.

Models four to nine each had one or more additional healthy humans located between the infected and back healthy human, referred to as the middle healthy human. The normalized air velocity surrounding this human was significantly increased in models four and six, as upwind flow promoted vertical turbulence. The normalized velocity surrounding the back healthy human ranged from 3.0 to 5.0, demonstrating an overall improvement to the divergence and convergence of the main airflow in each case. Overall, seating models two, four, and five increase eddy circulation, thus improving both the horizontal and vertical downwind flow.

This improved upwind and downwind airflow also helped decrease the average diameter of suspended droplets in all of the proposed seating arrangements, as shown in (Fig. 10). Models four, seven, and eight had the highest average diameter, approximately 30 μm; however, this still represents a reduction of the common model average diameter. The lowest average diameter, 2.80 μm, was found in seating model one, owing to the promoted localized airflow momentum and turbulence intensity. This decreased average diameter of suspended droplets contributes to the decline of droplet movement, which impacts COVID-19 transmission after a cough in each of the nine proposed seating arrangements.

The deposition fraction of expelled droplets within the first 0.40 s varied according to which human was coughing. When front human coughed, the deposition fraction generally decreased with time, as illustrated in (Fig. 11), thus decreasing the risk of COVID-19 transmission.

In model three, the overall deposition fraction was reduced from the baseline model by 27%; similarly, a 40% reduction was observed in models one and eight, and 47%, 52%, and 60% reductions were observed in models two, four, and five, respectively. In models seven and nine, however, the deposition fractions at 0.10 and 0.20 s were exceeded, leading to an overall increase in deposition fraction by 6%, thereby demonstrating poorer droplet dispersion owing to a lack of recirculation zones in the air vortex.

Regarding the middle human, the overall deposition fraction was below the common model value for each of the seating models proposed; further, the deposition fraction at each time point was also below the

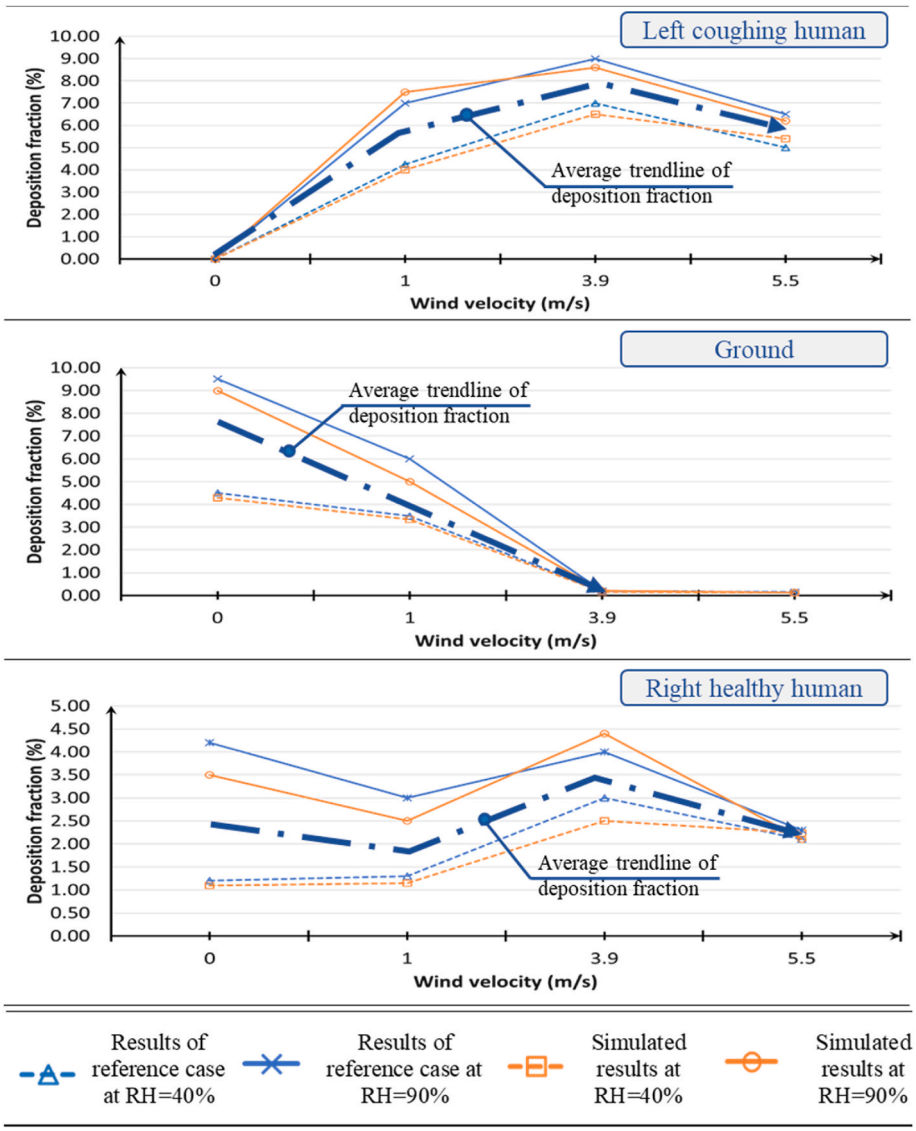

Fig. 8. Deposition fraction of verification study. Source the authors after [76].

common model value, except for that of model four at time $t = 0.10$ s. As a result, model four had a more modest overall reduction from the common model value (27%) than did models six, seven, eight, and nine (78%).

Similarly for the back human, the deposition fraction at each time point was below the common model value, except in models one and three at $t = 0.10$ s. Consequently, models three and one had a more modest decrease in droplet deposition fraction (30% and 35%, respectively) than did models seven (53%) and models two, four, five, six, eight, and nine (58%). This variation is due to the latter models having an enhanced dispersion of droplets owing to the turbulent airflows.

4. Discussion

Building upon the importance of urban seat design in COVID-19 transmission, the impact of seat configuration and backrest location and the limitations and potential implications of these results are discussed in this section.

4.1. Impact of design configurations

The proposed models can provide safer options for urban public seating, especially during the ongoing COVID-19 pandemic, due to the increased normalized air velocity and decreased deposition fraction and average droplet diameter of droplets expelled during a cough, as summarized in (Fig. 12). The diagonal linear configurations in models one, two, three, and four promoted recirculation regions through increased localized airflow momentum and turbulence intensity, which led to higher normalized air velocities, which confirmed in Refs. [64,70]. Furthermore, this also led to a decreased average droplet diameter and droplet deposition [76].

Small-diameter droplets cannot obtain sufficient momentum to conquer their inertia and disperse backward, as highlighted in Ref. [76]. Therefore, the high diameter values of coughing droplets receded, without proceeding with the backward recirculation flow. Additionally, the localized airflow momentum and turbulence intensity impacted the deposition fraction for both front, middle, and back humans. As the droplets cannot disperse backward, they rather dispersed toward the front coughing human, in line with a previous studies [105–107].

The performance of the centered configurations (i.e., models five to nine) varied according to the upwind design configuration. Models five, six, and nine allowed high normalized velocity and turbulence intensity; the smooth and curved configurations clearly impacted the local airflow velocities. In particular, the triangle configurations of models five and

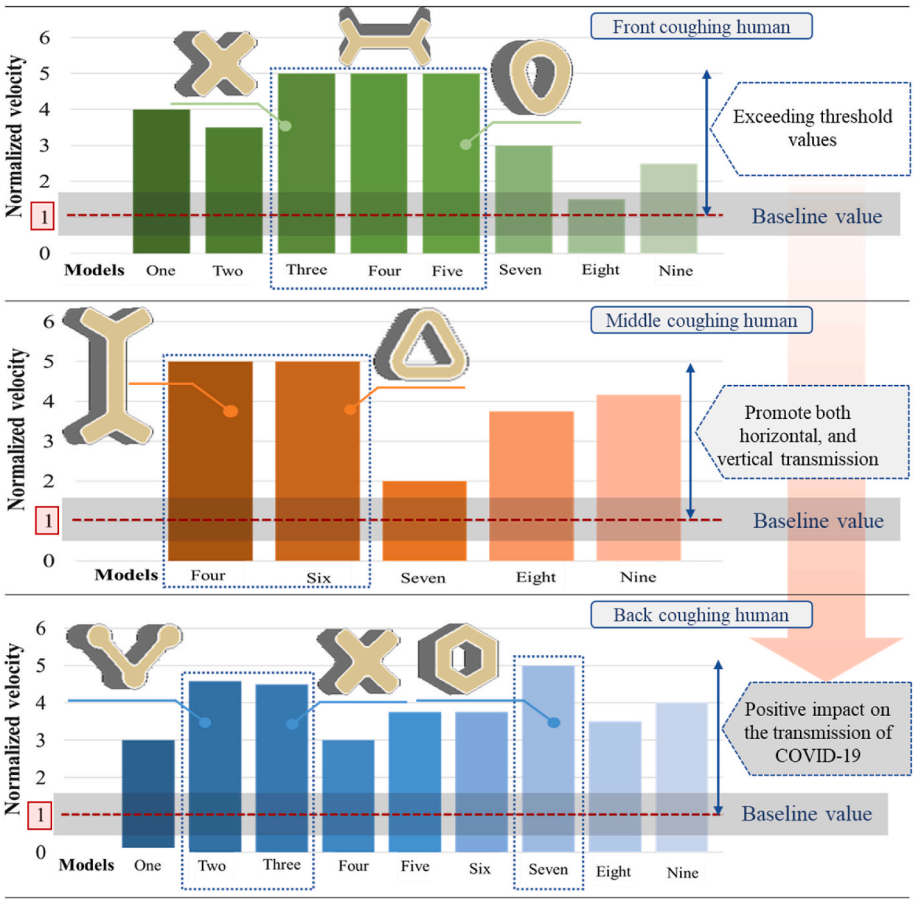

Fig. 9. Normalized air velocity of proposed seating models.

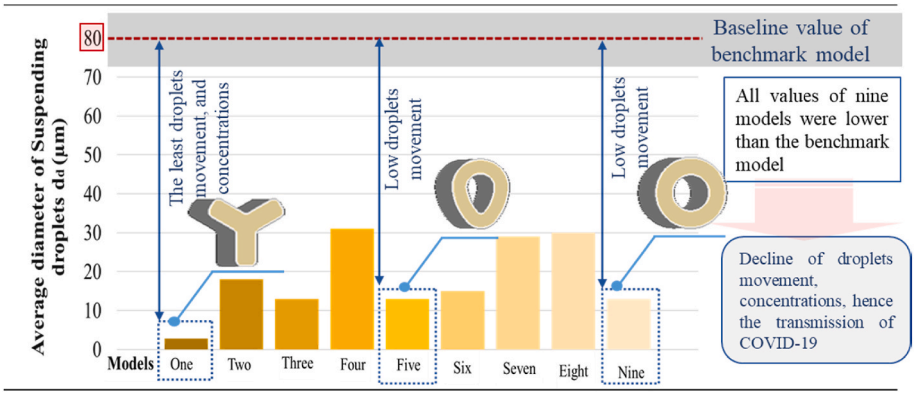

Fig. 10. Average diameter of suspending droplets.

six allowed for the main vortex and secondary eddies to be promoted, more so than the circular configuration of model nine. The polygonal configurations of models seven and eight showed a decreased local upwind airflow velocity near the front and middle humans; however, the secondary eddies increase the downward airflow velocity, which affects both the turbulence intensity and deposition faction.

The decreased average droplet diameter indicates that the droplets' momentum and energy were lower in the case of smooth and curved configurations, whereas in the case of the polygonal configurations of models seven and eight, the convection effect was promoted, thereby promoting their initial momentums.

Such variations impacted the deposition fraction, as the smooth and curved configurations allowed for a lower deposition fraction for the front, middle, and back humans in models five and six, and for the front and middle humans in model nine, where the droplets were dispersed backward. The polygonal configurations of models seven and eight allowed for a decrease in the deposition fraction because of the enhanced eddies, except for the back human in model seven owing to the decreased normalized velocity near the middle oblique edges.

4.2. *Impact of backrest place*

The location of the backrest place of urban seats was also demonstrated to impact the average droplet diameter and deposition fraction, and on the risk of COVID-19 transmission, as shown in (Fig. 13). The droplets expelled from a cough can more efficiently disperse when the

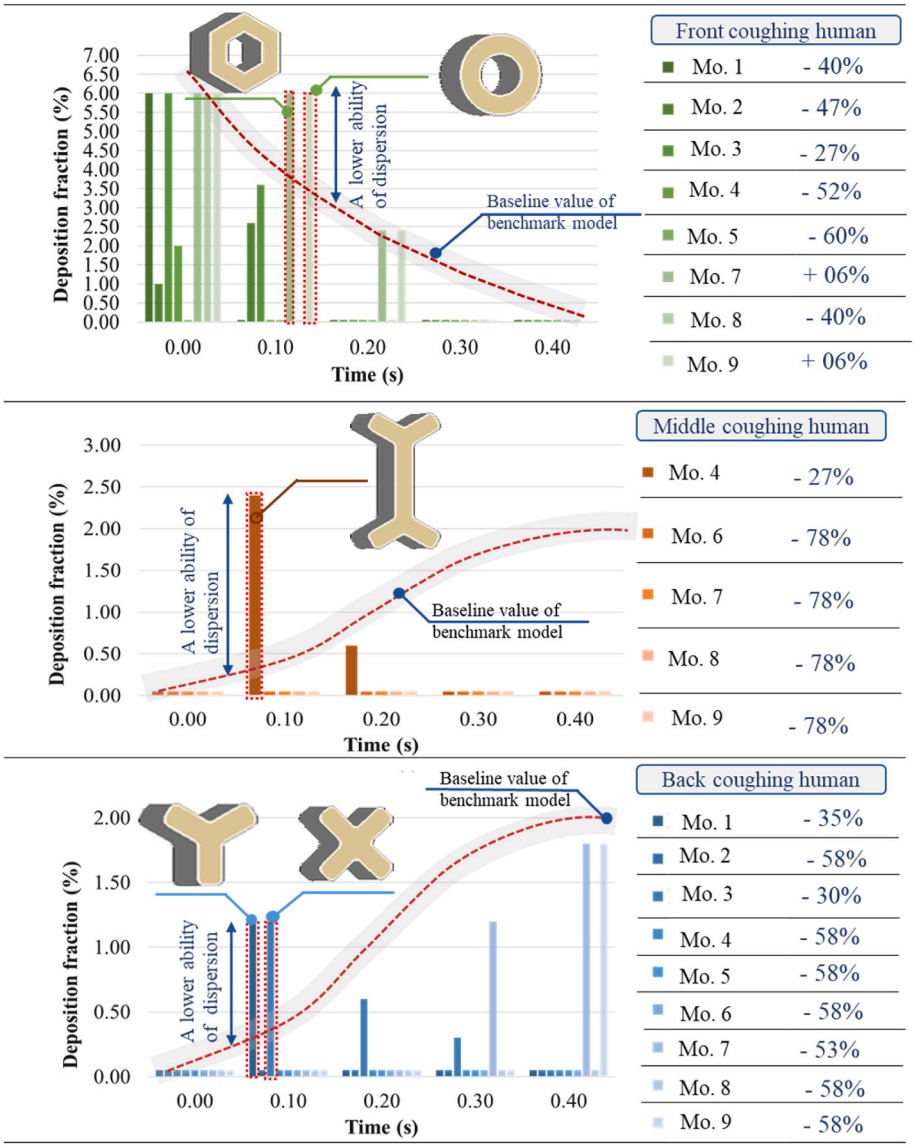

Fig. 11. Deposition fraction of proposed models.

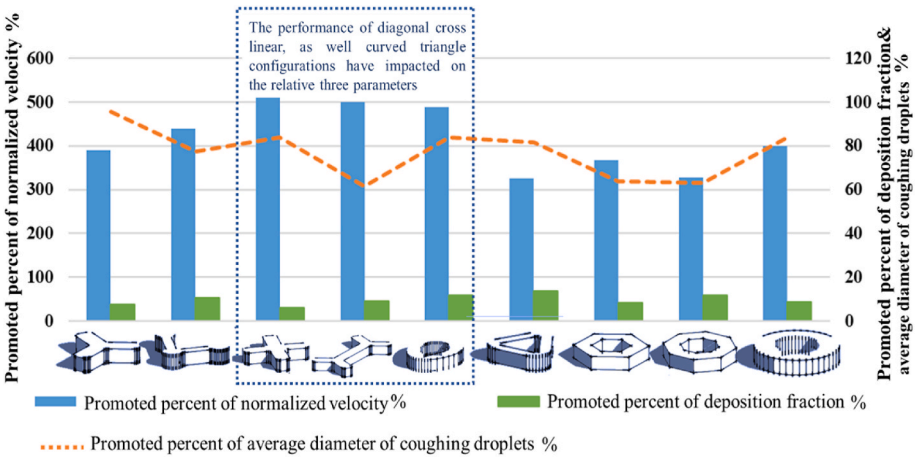

Fig. 12. The influence of seat configuration on the normalized air velocity, deposition fraction, and average droplet diameter.

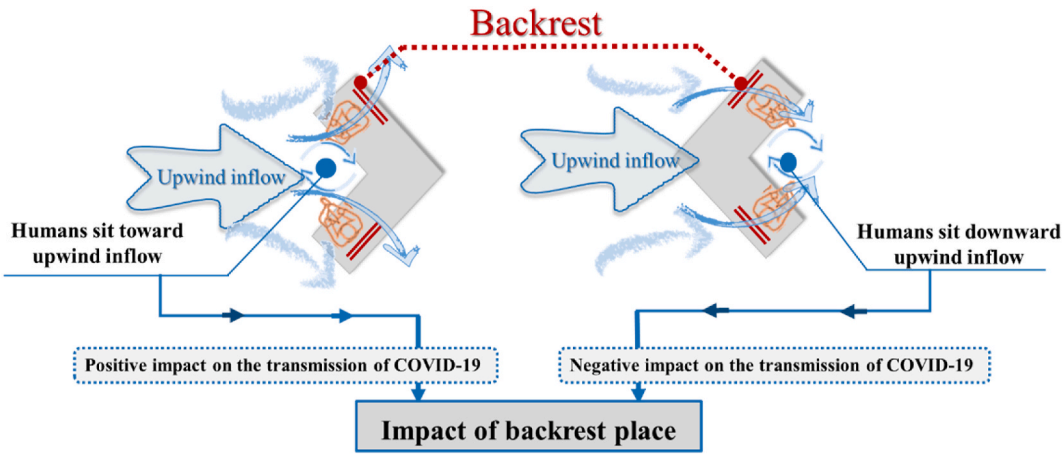

Fig. 13. The impact of backrests place on the transmission of COVID-19.

coughing human sits facing upwind. Whereas coughing human sits facing downwind, leads to larger droplets and increased deposition, due to their faster movement and higher droplet concentration; these larger droplets better maintain their initial momentum, owing to their relatively high Stokes number.

Further, backward backrests can enhance the magnitude of the velocity as well as the turbulence intensity in the recirculation zone. Such an enhancement can significantly promote crossing the main vortex, with secondary vortices divergence, and convergence of the shear layer vortices, besides shape the vertical turbulent velocities, as well turbulent diffusion, as indicated in Refs. [64,104].

4.3. Limitations

Here, the impact of urban seating configurations was examined under limited microclimate conditions. Moreover, a limited number of specific configurations were selected; further configurations can be developed according to the real microclimate conditions, local identity, urban context, and urban vibrancy. Although a small sample size was used that may not be generalized for all urban spaces, these findings offer a significant step toward developing urban seating configurations that allow residents safe outdoor socializing during a pandemic.

4.4. Potential implications

These findings help clarify the impact of urban seat design on viral transmission, which is particularly relevant during the ongoing COVID-19 pandemic. Such findings can be used to help improve urbanscape element design, which would allow for better urban ventilation and urban health. Improving the design of urbanscape elements can provide social resilience to encourage urban vibrancy, especially during the COVID-19 pandemic. Further, this can contribute to societal sustainability and thus offer social, psychological, economic, and quality-of-life benefits.

Furthermore, this work can contribute to the development of outdoor public spaces, by providing a framework for studying infection control mechanisms under microclimate conditions, in line with a previous study [20]. Urban planners, urbanscape specialists, policymakers, and corporate and public administrators are recommended to consider such infection control mechanisms to develop strategies and guidelines to promote urban health during the COVID-19 pandemic and decrease the possibility of viral infections in public spaces.

5. Conclusion

In this work, nine urban public seating designs, including diagonal linear, diagonal cross linear, and centered configurations, were proposed and analyzed based on a transient CFD model. A 3D Eulerian–Lagrangian method using the RNG k-epsilon turbulence model was validated to simulate and assess the proposed models based on the normalized air velocity, average droplet diameter, and droplet deposition fraction. The following conclusions were drawn.

- Models two, three, four, five, and six, with diagonal and tripartite form, allowed for the highest average normalized air velocity, which provides air vortex and thus affects the transmission of COVID-19. The lowest average diameter of suspended droplets was present in models one, three, and five, owing to the promoted localized airflow momentum and turbulence intensity, which contributed to a reduction of droplet movement and ambient air concentration. Furthermore, all proposed models demonstrated a decrease in the deposition fraction (>29% reduction); in particular, the deposition fraction was decreased by 68% when using models two, five, six, and eight.
- Each of the proposed models decreased the risk of viral transmission than the common model. In particular, the diagonal cross linear and curved triangle configurations demonstrated an improved airflow momentum and turbulent flow, decreasing the deposition of droplets expelled from a cough.
- The placement of backrests on urban seats can also impact viral transmission risk; as backward fixing backrests had a higher deposition fraction than did their frontal-fixed counterparts.

This work contributes to the design and development of urbanscape elements, especially public seating, which contributes to a healthy urban public environment. Investigations into this approach are ongoing to confirm such impacts during the COVID-19 pandemic.

Further efforts should emphasize detailed analyses of other urbanscape elements, such as shades or pergolas to investigate their impact on the transmission of COVID-19. The development or redesign of indoor public seats and natural ventilation mechanisms should also be investigated to provide healthy indoor spaces, as well. Such investigations into the design process of indoor and outdoor seating and socializing areas are necessarily interdisciplinary and require advanced wind tunnel investigations to validate such findings. Furthermore, such investigations can highlight the generative design to optimize such design process with various disciplines from architects, mechanical engineers, and software developers.

Funding

This research did not receive any specific grant from funding agencies in the public, commercial, or not-for-profit sectors.

Declaration of competing interest

The authors declare that they have no known competing financial interests or personal relationships that could have appeared to influence the work reported in this paper.

References

[1] K. Javanroodi, V. Nik, Interactions between extreme climate and urban morphology - investigating the evolution of extreme wind speeds from mesoscale to microscale, Urban Clim 31 (2020) 100544, https://doi.org/10.1016/j.uclim.2019.100544.

[2] K. Perini, A. Chokhachian, S. Dong, T. Auer, Modeling and simulating urban outdoor comfort: coupling ENVI-Met and TRNSYS by grasshopper, Energy Build. 152 (2017) 373–384, https://doi.org/10.1016/j.enbuild.2017.07.061.

[3] D. Kim, Exploratory study on the spatial relationship between emerging infectious diseases and urban characteristics: cases from Korea, Sustain. Cities Soc. 66 (2021) 102672, https://doi.org/10.1016/j.scs.2020.102672.

[4] A.M. Rahmani, S.Y.H. Mirmahaleh, Coronavirus disease (COVID-19) prevention and treatment methods and effective parameters: a systematic literature review, Sustain. Cities Soc. 64 (2021) 102568, https://doi.org/10.1016/j.scs.2020.102568.

[5] S. Sannigrahi, F. Pilla, B. Basu, A. Basu, A. Mölter, Examining the association between socio-demographic composition and COVID-19 fatalities in the European region using spatial regression approach, Sustain. Cities Soc. 62 (2020) 102418, https://doi.org/10.1016/j.scs.2020.102418.

[6] C. Zhou, F. Su, T. Pei, A. Zhang, Y. Du, B. Luo, Z. Cao, J. Wang, W. Yuan, Y. Zhu, C. Song, J. Chen, J. Xu, F. Li, T. Ma, L. Jiang, F. Yan, J. Yi, Y. Hu, Y. Liao, H. Xiao, COVID-19: challenges to GIS with big data, Geogr. Sustain. 1 (2020) 77–87, https://doi.org/10.1016/j.geosus.2020.03.005.

[7] Z. Ai, C.M. Mak, N. Gao, J. Niu, Tracer gas is a suitable surrogate of exhaled droplet nuclei for studying airborne transmission in the built environment, Build. Simul. 13 (2020) 489–496, https://doi.org/10.1007/s12273-020-0614-5.

[8] N. Dudalski, A. Mohamed, S. Mubareka, R. Bi, C. Zhang, E. Savory, Experimental investigation of far field human cough airflows from healthy and: influenza-infected subjects, Indoor Air 30 (2020) 966–977, https://doi.org/10.1111/ina.12680.

[9] Hao Xu, C. Yan, Q. Fu, K. Xiao, Y. Yu, D. Han, W. Wang, J. Cheng, Possible environmental effects on the spread of COVID-19 in China, Sci. Total Environ. 731 (2020) 139211, https://doi.org/10.1016/j.scitotenv.2020.139211.

[10] S. Li, S. Ma, J. Zhang, Association of built environment attributes with the spread of COVID-19 at its initial stage in China, Sustain, Cities Soc 67 (2021) 102752, https://doi.org/10.1016/j.scs.2021.102752.

[11] B. Li, Y. Peng, H. He, M. Wang, T. Feng, Built environment and early infection of COVID-19 in urban districts: a case study of Huangzhou, Sustain. Cities Soc. 66 (2021) 102685, https://doi.org/10.1016/j.scs.2020.102685.

[12] A. Das, S. Ghosh, K. Das, T. Basu, I. Dutta, M. Das, Living environment matters: unravelling the spatial clustering of COVID-19 hotspots in Kolkata megacity, India, Sustain. Cities Soc. 65 (2021) 102577, https://doi.org/10.1016/j.scs.2020.102577.

[13] M. Guo, P. Xu, T. Xiao, R. He, M. Dai, S.L. Miller, Review and comparison of HVAC operation guidelines in different countries during the COVID-19 pandemic, Build. Environ. 187 (2021) 107368, https://doi.org/10.1016/j.buildenv.2020.107368.

[14] L. von Seidlein, G. Alabaster, J. Deen, J. Knudsen, Crowding has consequences: prevention and management of COVID-19 in informal urban settlements, Build. Environ. 188 (2021) 107472, https://doi.org/10.1016/j.buildenv.2020.107472.

[15] K. Godri Pollitt, J. Peccia, A. Ko, N. Kaminski, C. Dela Cruz, D. Nebert, J. Reichardt, D. Thompson, V. Vasiliou, COVID-19 vulnerability: the potential impact of genetic susceptibility and airborne transmission, Hum. Genom. 14 (2020), https://doi.org/10.1186/s40246-020-00267-3.

[16] T. Jin, J. Li, J. Yang, J. Li, F. Hong, H. Long, Q. Deng, Y. Qin, J. Jiang, X. Zhou, Q. Song, C. Pan, P. Luo, SARS-CoV-2 presented in the air of an intensive care unit (ICU), Sustain. Cities Soc. 65 (2021) 102446, https://doi.org/10.1016/j.scs.2020.102446.

[17] B. Jones, P. Sharpe, C. Iddon, E.A. Hathway, C.J. Noakes, S. Fitzgerald, Modelling uncertainty in the relative risk of exposure to the SARS-CoV-2 virus by airborne aerosol transmission in well mixed indoor air, Build. Environ. 191 (2021) 107617, https://doi.org/10.1016/j.buildenv.2021.107617.

[18] Y. Li, H. Qian, J. Hang, X. Chen, P. Cheng, H. Ling, S. Wang, P. Liang, J. Li, S. Xiao, J. Wei, L. Liu, B.J. Cowling, M. Kang, Probable airborne transmission of SARS-CoV-2 in a poorly ventilated restaurant, Build. Environ. 196 (2021) 107788, https://doi.org/10.1016/j.buildenv.2021.107788.

[19] B. Blocken, T. van Druenen, T. Hooff, P.A. Verstappen, T. Marchal, L.C. Marr, Can indoor sports centers be allowed to re-open during the COVID-19 pandemic based on a certificate of equivalence? Build. Environ. 180 (2020) 107022, https://doi.org/10.1016/j.buildenv.2020.107022.

[20] B. Blocken, F. Malizia, T. van Druenen, T. Marchal, Towards Aerodynamically Equivalent COVID19 1.5 M Social Distancing for Walking and Running, 2020 (accessed June 30, 2020), www.urbanphysics.net/Social Distancing v20_White_Paper.pdf.

[21] L. Dietz, P. Horve, D. Coil, M. Fretz, J. Eisen, K. Wymelenberg, Novel Coronavirus (COVID-19) Outbreak: A Review of the Current Literature and Built Environment (BE) Considerations to Reduce Transmission, 2019, https://doi.org/10.20944/preprints202003.0197.v2, 2020.

[22] S. Bhattacharya, P.K. Reddy Maddikunta, Q.-V. Pham, T.R. Gadekallu, S. R. Krishnan S, C.L. Chowdhary, M. Alazab, M. Jalil Piran, Deep learning and medical image processing for coronavirus (COVID-19) pandemic: a survey, Sustain. Cities Soc. 65 (2021) 102589, https://doi.org/10.1016/j.scs.2020.102589.

[23] E. Brown, S. Kumar, T. Rajji, B. Pollock, B. Mulsant, Anticipating and mitigating the impact of COVID-19 pandemic on Alzheimer's disease and related dementias, Am. J. Geriatr. Psychiatr. 28 (2020) 712–721, https://doi.org/10.1016/j.jagp.2020.04.010.

[24] S. Ghosh, A. Das, T.K.H.S. Saha, B.P.A.M. Alamri, Impact of COVID-19 induced lockdown on environmental quality in four indian megacities using landsat 8 OLI and TIRS-derived data and mamdani fuzzy logic modelling approach, Sustainability 12 (2020) 5464–5476.

[25] J.Z. Zhou, Y. Qiu, Y. Pu, X. Huang, X.-Y. Ge, BioAider, An efficient tool for viral genome analysis and its application in tracing SARS-CoV-2 transmission, Sustain. Cities Soc. 63 (2020) 102466, https://doi.org/10.1016/j.scs.2020.102466.

[26] M.A. Rahman, N. Zaman, A.T. Asyhari, F. Al-Turjman, M.Z. Alam Bhuiyan, M. F. Zolkipli, Data-driven dynamic clustering framework for mitigating the adverse economic impact of Covid-19 lockdown practices, Sustain. Cities Soc. 62 (2020) 102372, https://doi.org/10.1016/j.scs.2020.102372.

[27] D. Toscano, F. Murena, The effect on air quality of lockdown directives to prevent the spread of SARS-CoV-2 pandemic in Campania Region—Italy: indications for a sustainable development, Sustainability 12 (2020) 5558, https://doi.org/10.3390/su12145558.

[28] M. Zivkovic, N. Bacanin, K. Venkatachalam, A. Nayyar, A. Djordjevic, I. Strumberger, F. Al-Turjman, COVID-19 cases prediction by using hybrid machine learning and beetle antennae search approach, Sustain. Cities Soc. 66 (2021) 102669, https://doi.org/10.1016/j.scs.2020.102669.

[29] B. Blocken, T. van Druenen, A. Ricci, L. Kang, T. van Hooff, P. Qin, L. Xia, C. A. Ruiz, J.H. Arts, J.F.L. Diepens, G.A. Maas, S.G. Gillmeier, S.B. Vos, A. C. Brombacher, Ventilation and air cleaning to limit aerosol particle concentrations in a gym during the COVID-19 pandemic, Build. Environ. 193 (2021) 107659, https://doi.org/10.1016/j.buildenv.2021.107659.

[30] WHO, Modes of Transmission of Virus Causing COVID-19: Implications for IPC Precaution Recommendations, 2020 accessed, https://www.who.int/news-room/commentaries/detail/modes-of-transmission-of-virus-causing-covid-19-implications-for-ipc-precaution-recommendations. (Accessed 17 July 2020).

[31] A. Sakharov, K. Zhukov, Study of an air curtain in the context of individual protection from exposure to Coronavirus (SARS-CoV-2) contained in cough-generated fluid particles, Physics 2 (2020) 340–351, https://doi.org/10.3390/physics2030018.

[32] N. Megahed, E.M. Ghoneim, Indoor Air Quality: rethinking rules of building design strategies in post-pandemic architecture, Environ. Res. 193 (2021) 110471, https://doi.org/10.1016/j.envres.2020.110471.

[33] W. Rice, T. Mateer, N. Reigner, P. Newman, B. Lawhon, D. Taff, Changes in recreational behaviors of outdoor enthusiasts during the COVID-19 pandemic: analysis across urban and rural communities, J. Urban Econ. 6 (2020) 1–7, https://doi.org/10.1093/jue/juaa020.

[34] M. Awada, B. Becerik-Gerber, S. Hoque, Z. O'Neill, G. Pedrielli, J. Wen, T. Wu, Ten questions concerning occupant health in buildings during normal operations and extreme events including the COVID-19 pandemic, Build. Environ. 188 (2021) 107480, https://doi.org/10.1016/j.buildenv.2020.107480.

[35] L.F. Pease, N. Wang, T.I. Salsbury, R.M. Underhill, J.E. Flaherty, A. Vlachokostas, G. Kulkarni, D.P. James, Investigation of potential aerosol transmission and infectivity of SARS-CoV-2 through central ventilation systems, Build. Environ. 197 (2021) 107633, https://doi.org/10.1016/j.buildenv.2021.107633.

[36] J. Honey-Rosés, I. Anguelovski, J. Bohigas, V. Chireh, C. Daher, C. Konijnendijk van den Bosch, J. Litt, V. Mawani, M. McCall, A. Orellana, E. Oscilowicz, H. U. Sánchez-Sepúlveda, M. Senbel, X. Tan, E. Villagomez, O. Zapata, M. Nieuwenhuijsen, The Impact of cOVID-19 on Public Space: A Review of the Emerging Questions, 2020, https://doi.org/10.31219/osf.io/rf7xa.

[37] Z. Jibiao, C. Ma, S. Dong, M. Zhang, Unconventional Prevention Strategies for Urban Public Transport in the COVID-19 Epidemic: Taking Ningbo City as a Case Study, 2020, https://doi.org/10.13140/RG.2.2.20856.06405.

[38] H. Li, C. Yc, H. Jx, C. Sw, Pilot study using telemedicine video-consultation for vascular patients' care during the COVID-19 period, Ann. Vasc. Surg. 68 (2020) 76–82, https://doi.org/10.1016/j.avsg.2020.06.023.

[39] A. Salama, Coronavirus Questions that Will Not Go Away: Interrogating Urban and Socio-Spatial Implications of COVID-19 Measures, 2020, https://doi.org/10.35241/emeraldopenres.13561.1.

[40] Will Cavendish, F. Cousins, Modelling a Changed World: Providing Expert Insight for COVID-19 Recovery Decisions, 2020 (accessed June 28, 2020), https://www.arup.com/perspectives/modelling-a-changed-world-providing-insight-for-covid-19-recovery-decisions#mainContact.

[41] A.R. Antony, R. Velraj, H. Fariborz, The contribution of dry indoor built environment on the spread of Coronavirus: data from various Indian states, Sustain. Cities Soc. 62 (2020) 102371, https://doi.org/10.1016/j.scs.2020.102371.

[42] J. Honey-Rosés, I. Anguelovski, V.K. Chireh, C. Daher, C. Konijnendijk van den Bosch, J.S. Litt, V. Mawani, M.K. McCall, A. Orellana, E. Oscilowicz, U. Sánchez, M. Senbel, X. Tan, E. Villagomez, O. Zapata, M.J. Nieuwenhuijsen, The impact of COVID-19 on public space: an early review of the emerging questions – design, perceptions and inequities, Cities Heal (2020) 1–17, https://doi.org/10.1080/23748834.2020.1780074.

[43] D. Elgheznawy, S. Eltarabily, Post-pandemic Cities - the Impact of COVID-19 on Cities and Urban Design, 10, 2020, pp. 75–84, https://doi.org/10.5923/j.arch.20201003.02.
[44] I. Ahmed, M. Ahmad, J.J.P.C. Rodrigues, G. Jeon, S. Din, A deep learning-based social distance monitoring framework for COVID-19, Sustain. Cities Soc. 65 (2021) 102571, https://doi.org/10.1016/j.scs.2020.102571.
[45] X. Fu, W. Zhai, Examining the spatial and temporal relationship between social vulnerability and stay-at-home behaviors in New York City during the COVID-19 pandemic, Sustain. Cities Soc. 67 (2021) 102757, https://doi.org/10.1016/j.scs.2021.102757.
[46] C. Sun, J. Zhai, The efficacy of social distance and ventilation effectiveness in preventing COVID-19 transmission, Sustain. Cities Soc. 62 (2020) 102390, https://doi.org/10.1016/j.scs.2020.102390.
[47] E. Ronchi, R. Lovreglio, EXPOSED: an Occupant Exposure Model for Confined Spaces to Retrofit Crowd Models during a Pandemic, 2020.
[48] A. Watterson, R. O'Neiill, Keep Your Distance: Is Two Metres Too Far or Not Far Enough to Protect from COVID-19 and Who Benefits and Who Loses if it Is Reduced ?, 2020, https://doi.org/10.13140/RG.2.2.17788.16008.
[49] A. El Mokadem, O. E Einen, N.A. Megahed, A.M. Hassan, Passive strategies of promoting outdoor air quality in microclimate, Int. J. Innov. Res. Sci. Eng. Technol. 8 (2019) 6966–6972, https://doi.org/10.15680/IJIRSET.2019.0806070.
[50] X. Wang, F. Liu, Z. Xu, Analysis of urban public spaces' wind environment by applying the CFD simulation method: a case study in Nanjing, Geogr. Pannonica. 23 (2019) 308–317, https://doi.org/10.5937/gp23-24249.
[51] L. Liu, Emerging study on the transmission of the Novel Coronavirus (COVID-19) from urban perspective: evidence from China, Cities 103 (2020) 102759, https://doi.org/10.1016/j.cities.2020.102759.
[52] M. Hu, J.D. Roberts, G.P. Azevedo, D. Milner, The role of built and social environmental factors in Covid-19 transmission: a look at America's capital city, Sustain. Cities Soc. 65 (2021) 102580, https://doi.org/10.1016/j.scs.2020.102580.
[53] N. Megahed, E. Ghoneim, Antivirus-built environment: lessons learned from Covid-19 pandemic, Sustain. Cities Soc. 61 (2020) 102350, https://doi.org/10.1016/j.scs.2020.102350.
[54] S. Tavares, D. Sellars, G. Mews, K. Dupre, C. Cândido, S. Towle, in: Editorial: Public Health and Well-Being in Public Open Spaces through Climate Responsive Urban Planning and Design, 5, 2020, pp. 1–6, https://doi.org/10.32891/jps.v5i2.1279.
[55] R. Greenwald, After COVID-19, What's Next for Landscape Architecture?, 2020. https://www.metropolismag.com/architecture/landscape/covid-19-landscape-architecture/.
[56] M. Sepe, Covid-19 pandemic and public spaces: improving quality and flexibility for healthier places, Urban Des. Int. 26 (2021) 159–173, https://doi.org/10.1057/s41289-021-00153-x.
[57] A. Jasiński, Public space or safe space – remarks during the COVID-19 pandemic, Tech. Trans. 117 (2020), https://doi.org/10.37705/techtrans/e2020020.
[58] M. Ahsan, Strategic decisions on urban built environment to pandemics in Turkey: lessons from COVID-19, J. Urban Manag. 9 (2020) 281–285, https://doi.org/10.1016/j.jum.2020.07.001.
[59] N. Gouveia, C. Kanai, Pandemics, cities and public health, Ambiente Sociedade 23 (2020), https://doi.org/10.1590/1809-4422asoc20200120vu2020l3id.
[60] K. Samuelsson, S. Barthel, J. Colding, G. Macassa, M. Giusti, Urban Nature as a Source of Resilience during Social Distancing amidst the Coronavirus Pandemic, 2020, https://doi.org/10.31219/osf.io/3wx5a.
[61] Bill Chaisson, The Lungs of the City, 2008 accessed, https://flowers4u.wordpress.com/2008/03/31/the-lungs-of-the-city/. (Accessed 20 August 2020).
[62] Justin Hollander, How Will COVID-19 Affect Public Spaces?, 2020 (accessed June 25, 2020), https://now.tufts.edu/articles/how-will-covid-19-affect-public-spaces.
[63] X. Xu, Y. Wu, W. Wang, T. Hong, N. Xu, Performance-driven optimization of urban open space configuration in the cold-winter and hot-summer region of China, Build. Simul. 12 (2018) 411–424, https://doi.org/10.1007/s12273-019-0510-z.
[64] A.M. Hassan, A.A. ELMokadem, N.A. Megahed, O.M. Abo Eleinen, Urban morphology as a passive strategy in promoting outdoor air quality, J. Build. Eng. 29 (2020) 101204, https://doi.org/10.1016/j.jobe.2020.101204.
[65] A.M. Hassan, A. El Mokadem, N.A. Megahed, O.M. Abo Eleinen, Improving outdoor air quality based on building morphology: numerical investigation, Front. Archit. Res. 9 (2020) 319–334, https://doi.org/10.1016/j.foar.2020.01.001.
[66] Y. Toparlar, B. Blocken, B. Maiheu, G.J.F. van Heijst, A review on the CFD analysis of urban microclimate, Renew. Sustain. Energy Rev. 80 (2017) 1613–1640, https://doi.org/10.1016/j.rser.2017.05.248.
[67] A. Cheshmehzangi, Multi-spatial environmental performance evaluation towards integrated urban design: a procedural approach with computational simulations, J. Clean. Prod. 139 (2016) 1085–1093, https://doi.org/10.1016/j.jclepro.2016.08.151.
[68] Z. Yuan, H. Yuanman, G. Chang, M. Liu, F. Shilei, W. Shizhe, Wang, Urban green space planning based on computational fluid dynamics model and landscape ecology principle: a case study of Liaoyang City, Northeast China, Chin. Geogr. Sci. 21 (2011), https://doi.org/10.1007/s11769-011-0488-7.
[69] D. Elgheznawy, S. Eltarabily, The impact of sun sail-shading strategy on the thermal comfort in school courtyards, Build. Environ. 202 (2021) 108046, https://doi.org/10.1016/j.buildenv.2021.108046.
[70] J. Leng, Q. Wang, K. Liu, Sustainable design of courtyard environment: from the perspectives of airborne diseases control and human health, Sustain. Cities Soc. 62 (2020) 102405, https://doi.org/10.1016/j.scs.2020.102405.
[71] C. Gromke, R. Buccolieri, S. Di Sabatino, B. Ruck, Dispersion study in a street canyon with tree planting by means of wind tunnel and numerical investigations – evaluation of CFD data with experimental data, Atmos. Environ. 42 (2008) 8640–8650, https://doi.org/10.1016/j.atmosenv.2008.08.019.
[72] A.P.R. Jeanjean, G. Hinchliffe, W.A. McMullan, P.S. Monks, R.J. Leigh, A CFD study on the effectiveness of trees to disperse road traffic emissions at a city scale, Atmos. Environ. 120 (2015) 1–14, https://doi.org/10.1016/j.atmosenv.2015.08.003.
[73] S. Vranckx, P. Vos, OpenFOAM CFD Simulation of Pollutant Dispersion in Street Canyons: Validation and Annual Impact of Trees, 2013.
[74] Z. Zhang, Q. Chen, Experimental measurements and numerical simulations of particle transport and distribution in ventilated rooms, Atmos, Environ. Times 40 (2006) 3396–3408, https://doi.org/10.1016/j.atmosenv.2006.01.014.
[75] B. Zhao, C. Yang, X. Yang, S. Liu, Particle dispersion and deposition in ventilated rooms: testing and evaluation of different Eulerian and Lagrangian models, Build. Environ. 43 (2008) 388–397, https://doi.org/10.1016/j.buildenv.2007.01.005.
[76] Y. Feng, T. Marchal, T. Sperry, H. Yi, Influence of wind and relative humidity on the social distancing effectiveness to prevent COVID-19 airborne transmission: a numerical study, J. Aerosol Sci. 147 (2020) 105585, https://doi.org/10.1016/j.jaerosci.2020.105585.
[77] H. Montazeri, B. Blocken, J.L.M. Hensen, CFD analysis of the impact of physical parameters on evaporative cooling by a mist spray system, Appl. Therm. Eng. 75 (2015) 608–622, https://doi.org/10.1016/j.applthermaleng.2014.09.078.
[78] R. Sureshkumar, S.R. Kale, P.L. Dhar, Heat and mass transfer processes between a water spray and ambient air – II. Simulations, Appl. Therm. Eng. 28 (2008) 361–371, https://doi.org/10.1016/j.applthermaleng.2007.09.015.
[79] X. Li, Y. Shang, Y. Yan, L. Yang, J. Tu, Modelling of evaporation of cough droplets in inhomogeneous humidity fields using the multi-component Eulerian-Lagrangian approach, Build. Environ. 128 (2018) 68–76, https://doi.org/10.1016/j.buildenv.2017.11.025.
[80] X. Chen, Y. Feng, W. Zhong, C. Kleinstreuer, Numerical investigation of the interaction, transport and deposition of multicomponent droplets in a simple mouth-throat model, J. Aerosol Sci. 105 (2017) 108–127, https://doi.org/10.1016/j.jaerosci.2016.12.001.
[81] Y. Feng, C. Kleinstreuer, A. Rostami, Evaporation and condensation of multicomponent electronic cigarette droplets and conventional cigarette smoke particles in an idealized G3–G6 triple bifurcating unit, J. Aerosol Sci. 80 (2015) 58–74, https://doi.org/10.1016/j.jaerosci.2014.11.002.
[82] A. Haghnegahdar, J. Zhao, Y. Feng, Lung aerosol dynamics of airborne influenza A virus-laden droplets and the resultant immune system responses: an in silico study, J. Aerosol Sci. 134 (2019) 34–55, https://doi.org/10.1016/j.jaerosci.2019.04.009.
[83] N. Guerrero, J. Brito, P. Cornejo, COVID-19. Transport of Respiratory Droplets in a Microclimatologic Urban Scenario, 2020, https://doi.org/10.1101/2020.04.17.20064394.
[84] M. Brown, R. Lawson, D. DeCroix, R. Lee, COMPARISON OF CENTERLINE VELOCITY MEASUREMENTS OBTAINED AROUND 2D AND 3D BUILDING ARRAYS IN A WIND TUNNEL, 2001.
[85] N. Dudalski, A. Mohamed, E. Savory, S. Mubareka, Experimental Measurements of Far Field Cough Airflows Produced by Healthy and Influenza-Infected Subjects, 2018, https://doi.org/10.25071/10315/35362.
[86] H. Nishimura, S. Sakata, A. Kaga, A New methodology for studying dynamics of aerosol particles in sneeze and cough using a digital high-vision, high-speed video system and vector analyses, PloS One 8 (2013), e80244, https://doi.org/10.1371/journal.pone.0080244.
[87] J. Li, X. Cao, J. Liu, C. Wang, Z. yz, Global airflow field distribution in a cabin mock-up measured via large-scale 2D-PIV, Build. Environ. 93 (2015) 234–244, https://doi.org/10.1016/j.buildenv.2015.06.030.
[88] X. Cao, J. Liu, J. Pei, Y. Zhang, J. Li, X. Zhu, 2D-PIV measurement of aircraft cabin air distribution with a high spatial resolution, Build. Environ. 82 (2014) 9–19, https://doi.org/10.1016/j.buildenv.2014.07.027.
[89] Y. Yan, X. Li, L. Yang, P. Yan, J. Tu, Evaluation of cough-jet effects on the transport characteristics of respiratory-induced contaminants in airline passengers' local environments, Build. Environ. 183 (2020), https://doi.org/10.1016/j.buildenv.2020.107206.
[90] The Conversation, How Cities Can Add Accessible Green Space in a Post-coronavirus World, 2020 (accessed June 25, 2020), https://theconversation.com/how-cities-can-add-accessible-green-space-in-a-post-coronavirus-world-139194.
[91] A. Zhang, W. Li, J. Wu, J. Lin, J. Chu, C. Xia, How can the urban landscape affect urban vitality at the street block level? A case study of 15 metropolises in China, Environ. Plann. Plann. Des. (2020), https://doi.org/10.1177/2399808320924425.
[92] A. Chatzidimitriou, S. Yannas, Microclimate design for open spaces: ranking urban design effects on pedestrian thermal comfort in summer, Sustain. Cities Soc. 26 (2016) 27–47, https://doi.org/10.1016/j.scs.2016.05.004.
[93] E. Higueras, E. Román, J. Fariña, in: J. Martinez, C.A. Mikkelsen, R. Phillips (Eds.), Guidelines for Healthier Public Spaces for the Elderly Population: Recommendations in the Spanish Context BT - Handbook of Quality of Life and Sustainability, Springer International Publishing, Cham, 2021, pp. 35–51, https://doi.org/10.1007/978-3-030-50540-0_3.
[94] S. Sun, X. Xu, Z. Lao, W. Liu, Z. Li, E. Higueras García, L. He, J. Zhu, Evaluating the impact of urban green space and landscape design parameters on thermal

comfort in hot summer by numerical simulation, Build. Environ. 123 (2017) 277–288, https://doi.org/10.1016/j.buildenv.2017.07.010.
[95] X. Xu, S. Sun, W. Liu, E.H. García, L. He, Q. Cai, S. Xu, J. Wang, J. Zhu, The cooling and energy saving effect of landscape design parameters of urban park in summer: a case of Beijing, China, Energy Build. 149 (2017) 91–100, https://doi.org/10.1016/j.enbuild.2017.05.052.
[96] Filippo Bazzoni, Guilia Boni, Rawad Choubassi, Dante Presicce, Access to Green Areas and Public Realm: the Case of Milan, 2020.
[97] A. El Mokadem, O. El Einen, N.A. Megahed, A. Hassan, Analytical trends of building morphology as a passive strategies to promote outdoor air quality, Int. J. Innov. Res. Sci. Eng. Technol. 8 (2019) 6944–6952.
[98] S. Emeis, K. Baumann-Stanzer, M. Piringer, M. Kallistratova, R. Kouznetsov, V. Yushkov, Wind and turbulence in the urban boundary layer - analysis from acoustic remote sensing data and fit to analytical relations, Meteorol. Z. 16 (2007) 393–406, https://doi.org/10.1127/0941-2948/2007/0217.
[99] I.P. Castro, H. Cheng, R. Reynolds, Turbulence over urban-type roughness: deductions from wind-tunnel measurements, Boundary-Layer Meteorol. 118 (2006) 109–131, https://doi.org/10.1007/s10546-005-5747-7.
[100] M. Jicha, J. Pospisil, Influence of vehicle-induced turbulence on pollutant dispersion in street canyon and adjacent urban area, Int. J. Environ. Pollut. 62 (2017) 89, https://doi.org/10.1504/IJEP.2017.10010368.
[101] K. Ahmad, M. Khare, K.K. Chaudhry, Wind tunnel simulation studies on dispersion at urban street canyons and intersections—a review, J. Wind Eng. Ind. Aerod. 93 (2005) 697–717, https://doi.org/10.1016/j.jweia.2005.04.002.
[102] J. Franke, A. Hellsten, H. Schlünzen, B. Carissimo, The COST 732 best practice guideline for CFD simulation of flows in the urban environment: a summary, Int. J. Environ. Pollut. 44 (2011) 419–427, https://doi.org/10.1504/IJEP.2011.038443.
[103] J. Hang, Z. Luo, M. Sandberg, J. Gong, Natural ventilation assessment in typical open and semi-open urban environments under various wind directions, Build. Environ. 70 (2013) 318–333, https://doi.org/10.1016/j.buildenv.2013.09.002.
[104] C. Yuan, E. Ng, L.K. Norford, Improving air quality in high-density cities by understanding the relationship between air pollutant dispersion and urban morphologies, Build. Environ. 71 (2014) 245–258, https://doi.org/10.1016/j.buildenv.2013.10.008.
[105] K.H. Chan, J.S.M. Peiris, S.Y. Lam, L.L.M. Poon, K.Y. Yuen, W.H. Seto, The effects of temperature and relative humidity on the viability of the SARS coronavirus, Adv. Virol. 2011 (2011) 734690, https://doi.org/10.1155/2011/734690.
[106] D. Leslie, H.P. F, C.D. A, F. Mark, E.J. A, V.D.W. Kevin, G.J. A, Novel coronavirus (COVID-19) pandemic: built environment considerations to reduce transmission, mSystems 5 (2021) (2019), https://doi.org/10.1128/mSystems.00245-20 e00245-20.
[107] S.W. Kim, M.A. Ramakrishnan, P.C. Raynor, S.M. Goyal, Effects of humidity and other factors on the generation and sampling of a coronavirus aerosol, Aerobiologia 23 (2007) 239–248, https://doi.org/10.1007/s10453-007-9068-9.